

Behavior of T-Beams Under Cyclic Displacement Reversals

Nicolas El-Joukhadar¹, H. E. Zerbe² and S. J. Pantazopoulou³

¹PhD Student, Department of Civil Engineering, Lassonde Faculty of Engineering, York University, Toronto, Ontario, Canada

²Associate Professor, Department of Civil Engineering, Faculty of Engineering, University of Balamand, Koura, Lebanon

³Professor, Department of Civil Engineering, Lassonde Faculty of Engineering, York University, Toronto, Ontario, Canada

ABSTRACT

This paper investigates the response of T-beams under reversed cyclic displacement simulating earthquake effects on reinforced concrete (RC) frames. The study includes a series of experiments conducted on specimens and nonlinear finite element correlation of the experimental study in order to obtain insights in important response aspects such as spread of yielding in the plastic hinge zone, and web to flange interaction in hogging and sagging moments. The project involved five beams tested under four-point loads applied under displacement control according with a mid-span displacement cyclic history of increasing displacements; parameters of the study were, the shear reinforcement amounts provided in the potential plastic hinge zone, and the external confinement provided through CFRP wraps in the constant moment region (plastic zone) – one and two plies and strip arrangements were considered as alternatives. The role of confinement in relocating the plasticity region through its effect on bond was observed in the tests and is reproduced using advanced nonlinear finite element modeling of the experiments (using the ATENA software); the kinematics of flange-beam interaction with increasing drift is illustrated by the model to be particularly relevant over the shear span. The experimental results are corroborated with the model and with particular emphasis on the mechanics of yield penetration beyond the nominal plastic hinge region.

Keywords: T-beams, plastic hinge length, yield penetration, CFRP jackets, Finite Elements.

INTRODUCTION

A series of experiments on beams were conducted to establish the effect of different forms of detailing on the rotation capacity and the spread of the plastic hinge region during reversed cyclic loading over the beam shear span (i.e. the distance from peak moment to the support point, see Figure 1. Through the experiment it was possible to study the effect of unrestrained buckling in the highly inelastic regions on the subsequent response of the reinforcement in the plastic hinge areas, the penetration of strain beyond the areas of nominal yielding, and the ability of advanced FE modeling to reproduce the experimental trends. To this end, nonlinear 3-D modeling of the structure (using brick elements for concrete, truss elements for the reinforcement and pertinent bond links) were used to idealize the structural system. Figure 1 depicts the idealized relationship between a beam in

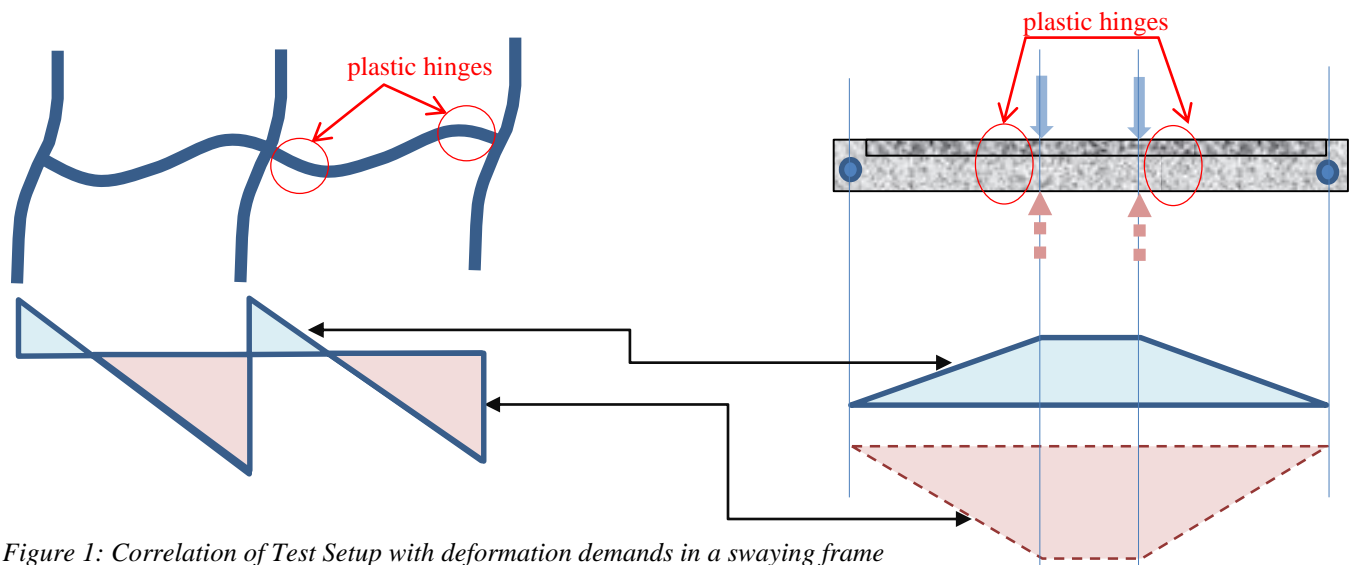


Figure 1: Correlation of Test Setup with deformation demands in a swaying frame

a moment resisting frame under lateral displacement reversals simulating earthquake effects and the typical shear span of the test conducted. In promoting the plastic hinge next to the constant moment region, in the shear-span, the central constant moment region of the specimen corresponds to the highly confined zone of a column where the longitudinal reinforcement of the beam shear span may be considered fully developed. Through the tests and the analysis, it is possible to observe the evolution of the plastic hinge region in the shear spans and the interaction between the beam web and the monolithically connected slab.

EXPERIMENTAL PROGRAM

Specimens

The experimental program consisted of testing five T-beams at half scale under reversed cyclic displacements. The beams were pin-supported in the ends and were tested under symmetric, displacement-controlled conditions, through two intermediate loading points acting at the third points of the span as depicted in Figures 1 and 2. Therefore, throughout the load history the central region (800 mm long) was under a constant moment, which was intended to enforce a constant shear state over the outside thirds of the span length up to the end pins. The total length of the beams was 3m, but the clear span between end-pins was 2.75m. The shear span was 975 mm on each side of the constant moment region (which was 800mm long), whereas the beam extended beyond the supports by 125 mm.

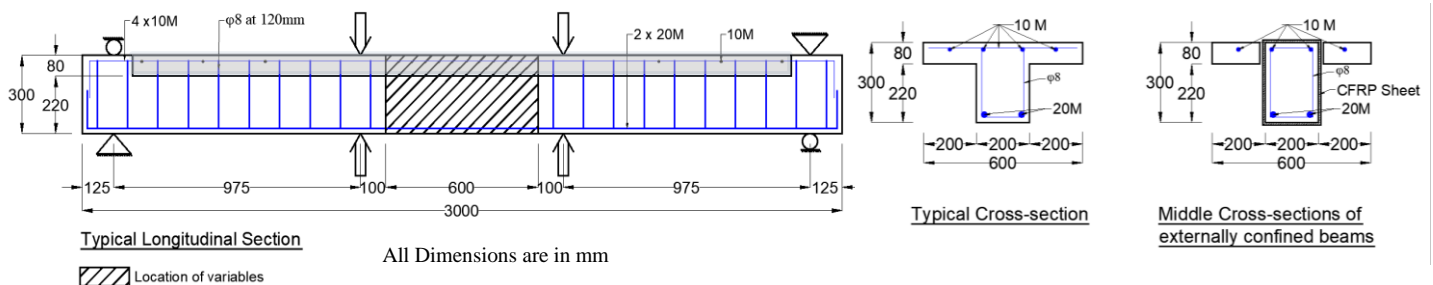
Typical beam cross-section and longitudinal reinforcement arrangement are depicted in Figure 2. Cross sections were 300mm high by 200mm wide, and were monolithically cast with an 80mm thick slab, which extended over the length of the beam specimen up to a distance of 200 mm from the end supports; the slab extended symmetrically 200mm on each side of the web resulting in a transverse slab width of 600mm. A parameter of study was the amount of confinement available in the central (constant moment region) which, in the experiment, was the designated region of extended yielding. Confinement was provided either in the form of stirrups or through FRP jacketing (by transverse wrapping of CFRP sheets around the beam web along 600mm of the constant moment region – this was achieved by cutting a slit longitudinally at the point of contact between slab and beam web thereby introducing a discontinuity between the two elements, to the extent that in that region the beam was effectively a rectangular section). Table 1 shows the beam variables.

Table 1 Beam Variables

Beam ID	B1	B2	B3	B4	B5
Stirrup anchorage	By 90° hooks	By 135° hooks	As B1	As B1	As B1
Internal Confinement in the constant moment region	8 mm diameter stirrups spaced at 120mm o.c.	8 mm diameter stirrups spaced at 60mm o.c.	As B1	As B1	As B1
CFRP jacketing	-	-	2 plies fully wrapped	1 ply fully wrapped	Two 200mm wide strips
Concrete Strength, f_c' - MPa ⁴	25.7	25.3	26.3	27.4	27.2

⁴ Values reported are the averages of three cylinder compressive strengths tested at the day of the respective beam experiment. All beams were cast the same day from the same batch having a strength of 19.5 MPa at 28 days.

Outside the constant moment region, in the shear spans, the stirrups were spaced at 120 mm o.c. with a clear concrete cover of 20mm. Bottom reinforcement comprised two bars ($D_b=20\text{mm}$), top reinforcement comprised four bars ($D_b=12\text{mm}$) and $\Phi=8.1$ mm smooth bars were used as transverse (stirrup) reinforcement (beam effective depth in sagging moment, $d=300-20-8-$



10=262mm; 267mm for hogging). Three transverse bars ($D_b=12\text{mm}$) were also placed in the shear spans over the entire width of slab as connection reinforcement with the beam web. Slab was unconnected with the beam web in the central region.

Confinement in Beam B2 was designed for special moment resisting frames as described by [1]. Material properties for the reinforcement and the CFRP wraps are given in Table 2.

Test Setup

The setup shown in Figure 3 was designed to facilitate the application of displacement either in the upwards or in the downwards direction during the cyclic displacement reversals. The spreader loading points were symmetrically placed about the beam midspan as depicted in Figure 2. Displacements were imposed through loading plates which acted on the beam web only (the loading plates were bearing through half cylinders that were attached both at the top and the bottom of the beam and secured through external post-tensioned rods, as depicted in Figure 3).



Figure 3 Test Setup

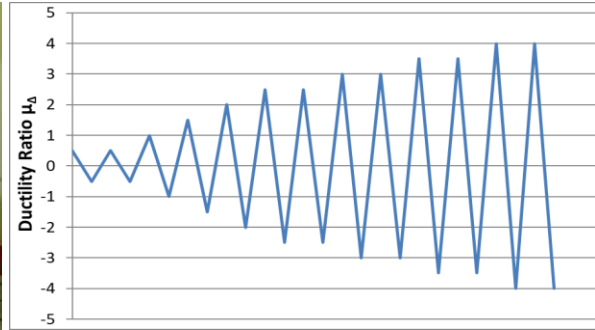


Figure 4 Loading History

Table 2 Rebar and CFRP Properties

Material Name	Density ρ_f (g/cm^3)	Diameter d_b / Thickness t_f (mm)	Yield Strength f_y (MPA)	Tensile Strength f_{fr}/f_u (MPA)	Tensile Modulus E_f (MPA)	Ultimate Tensile Strain ϵ_{fr}
Sika Wrap 231c	1.82	0.129	-	4900	230000	0.017
$\Phi 8$	-	8.1	327	440	200000	0.16
$D_b=12\text{mm}$	-	11.9	519	614	200000	0.12
$D_b=20\text{mm}$	-	19.95	550	679	200000	0.16

Displacement History

Figure 4 plots the history of applied displacement reversals during the test. Displacement amplitudes are given as multiples of the measured yield displacement of the specimen in the direction of loading, so the numbers listed are actually measures of displacement ductility demand, μ_{Δ} . Three loading rates were used as follows: between $\mu_{\Delta}=1$ and $\mu_{\Delta}=2$ the loading rate was 0.2 mm/s; between $\mu_{\Delta}=2.5$ and $\mu_{\Delta}=3$ the loading rate was 0.4 mm/s and from $\mu_{\Delta}=3.5$ onwards, the loading rate was increased to 0.8 mm/s.

Test Results

Figure 5 plots the Moment-curvature relationship for two sections, i.e., 1) a rectangular section (separated through slits from the slab), which represents the constant moment region reinforced with two 12mm-diameter top bars and two 20mm diameter bottom bars, and 2) the T-section which represents the member in the shear span, reinforced with four 12mm diameter bars as top reinforcement and two 20mm diameter bars as bottom reinforcement. The hogging moment capacity of the rectangular section (in the central region) was about 50% of that in the adjacent shear span; a reduction to this level was observed in the experimental testing as soon as the isolated unconfined slab strips outside the slits fractured in compression. Owing to this detail the flexural strength envelopes along the beam lengths are as shown in Figure 6. Theoretically, this means that inelasticity ought to be contained within the central region where even after CFRP jacketing flexural strength was but mildly affected, whereas the shear spans should remain intact since the flexural moment applied to yield the central region would always be below the respective yield strengths of the adjacent sections, according to Figure. 6.

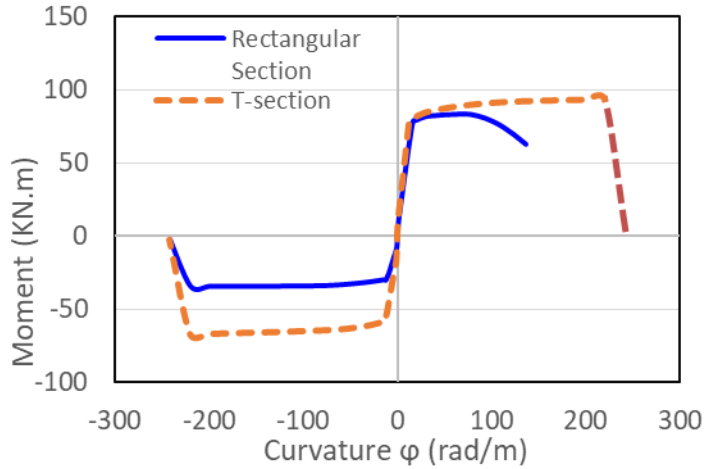


Figure 5 Moment-Curvature Diagrams of the constant moment and shear span sections.

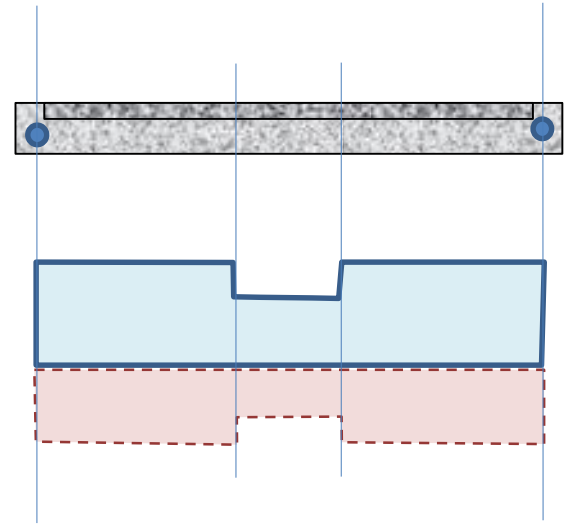


Figure 6 Flexural Strength Envelope (blue = sagging, red = hogging)

This was confirmed during testing of beams B1 and B2 which developed intense reinforcement yielding in the central region whereas the adjacent shear spans developed elastic response. In the end, failure was contained in the constant moment region, and it was manifested by disintegration of concrete in the slab in that segment, followed by buckling of longitudinal bars (only for beam B1), crushing of concrete and finally bar rupture. In the case of beam B2, due to the closer spacing of stirrups in the central 600mm highly confined region, longitudinal bars were only able to buckle right outside of the confined region as shown in Figure 8(b). Stirrups of beam B2 had 135° bent hooks that did not open during the large displacement cycles delaying buckling of longitudinal bars as opposed to the 90° bent hooks that opened up in the rest of the beams as soon as bars buckled, see Figures 8. Beams B3, B4 and B5 showed a much more extensive region of inelasticity despite the strength envelope of Fig. 6, starting in the constant moment region and extending into the shear span. Although tension cracks initiated in the midspan,

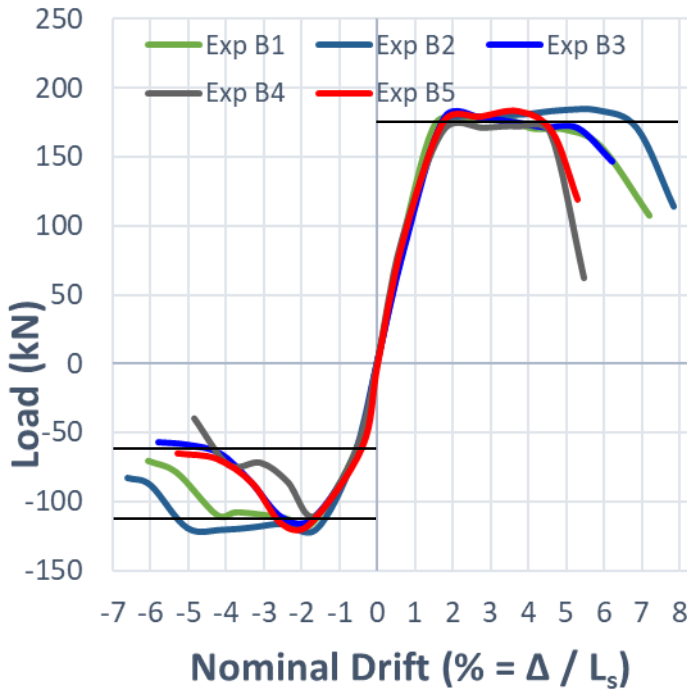


Figure 7 Backbone Curves of Experimental Hysteretic Loops of Beams 1 to 5

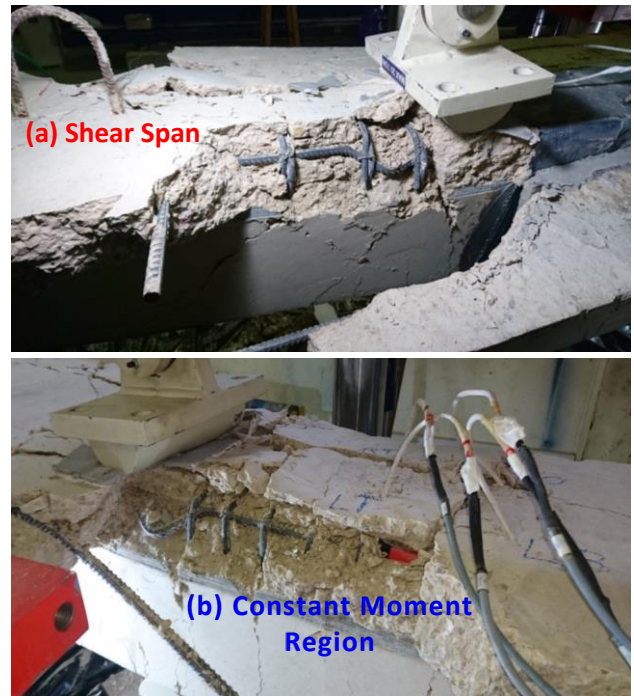


Figure 8 (a) Buckling of top bars in beam B3, (b) Buckling of top bars in beam B2

failure occurred in the shear span as shown in Figure 8(a). This type of failure started by disintegration of the slab in the shear span, buckling of top web reinforcement, crushing of concrete and finally rupture of the previously buckled bars.

It was observed that for beams externally confined with FRP, yield penetration of bar strains, bar buckling and eventual rupture in the adjacent shear spans controlled the specimen failure despite the strength difference between the central and shear spans as depicted in Figure 6. Figure 7 plots the backbone curves of the hysteretic loops of the five beams from the experimental program. Also shown are horizontal lines that represent the flexural strengths calculated from the moment curvature analysis using the actual material properties. To understand the important role of yield penetration and the significance of bond strength in the FRP-confined as compared to the conventionally confined shear span, detailed F.E. analysis of the specimens was undertaken as summarized in the following sections.

FINITE ELEMENT ANALYSIS

Finite Element Modeling

Modeling of the beams was conducted using the Finite Element platform ATENA [2]. Two types of beams were modeled, T-beams and rectangular beams. T-beams were used to analyze the diagonal crack pattern developed in the flange, the remaining parts of the specimens were modeled as having a rectangular section: the two longitudinal 12mm diameter bars that belonged to the flanges were assigned a bond model with a very low bond strength. Only half of the specimen lengths of B1 and B2 were modeled on account of symmetry in both setup and observed response, whereas in the case of the other specimens (beams B3, B4 and B5) the entire lengths were modeled because asymmetric behavior was observed during experimental testing of these beams.

Material Properties

Concrete behavior was modeled using the material model “3D Nonlinear Cementitious2” in ATENA. The model considers a biaxial strength failure envelope under plane stress. The nonlinear behavior of concrete in the biaxial stress state is defined by an effective uniaxial stress based on the corresponding uniaxial strain in principal directions. The material was assigned the measured properties for the modulus of Elasticity E_c , the concrete compressive strength f_c' , and the tensile strength f_t . The Specific Fracture Energy was taken equal to $G_f = 1.2 E^{-4}$ MN/m, tension stiffening coefficient $C_{ts}=0.1$ and the unloading factor=0.05. Default values were used for the other parameters as per the ATENA manual. Reinforcing bars were modeled as truss elements using the “Cyclic Reinforcement” model [2] and were assigned the corresponding modulus of Elasticity E_s , yield stress f_y , ultimate stress f_u , and maximum (rupture) strain ϵ_{lim} . The Menegotto-Pinto parameters used for the hysteresis loops were, $R=5$, $C_1=30$ and $C_2=0.15$ to model the behavior seen in the experiments. Default values were used for all other variables of the Menegotto-Pinto Model [2]. Interface contact between loading plate and concrete was modeled as a 3D interface with no shear and tensile strength so as to allow relative lateral displacement between the plate and the beam. The properties of bond of the reinforcement in the web were calculated according with the FIB model code 2010 [3] (favorable bond) with $\tau_{max}=6.3$ MPa, $\tau_{res}=2.5$ MPa, $s_1=1$ mm, $s_2=3$ mm and $s_3=12$ mm whereas the bond material for bars in unconfined concrete were modeled following the FIB model 2010[3] (unfavorable bond) with $\tau_{max}=5$ MPa, $\tau_{res}=0.7$ MPa, $s_1=0.6$ mm, $s_2=0.6$ mm and $s_3=2.5$ mm. CFRP wraps were modeled as discrete reinforcing bars with bi-linear behavior having the corresponding modulus of elasticity E_f , and yield strength f_f and were placed on the face of concrete around the cross-section.

Macro-Elements and Reinforcement

Meshing refers to a Cartesian coordinate system where x is along the longitudinal direction of the beam, z is in the vertical direction (displacement axis) and y is along the weak axis of the beam web cross section. Half of the total length of beams B1 and B2 were modeled ($u_x=0$ at midspan); this half was further divided lengthwise in two symmetric macro-elements through the centroidal axis of the members (plane $z=0$, $u_z=0$); beams B3, B4 and B5 were modeled as four macro elements, in order to obtain a finer mesh in the CFRP-jacketed region. Longitudinal reinforcement was embedded with the corresponding hooks at the supports and had a no slip condition at the midspan for beams B1 and B2. For beams B3, B4 and B5, the respective bond model was assigned along the bar outside the CFRP-jacketed zone. Perfect reinforcement-concrete bond was considered over the jacketed length to represent the effect of confinement on bond strength. Flange longitudinal bars were assigned the weaker bond model and did not have any hooks. Stirrups were modeled with the actual hooks and bends, and were in perfect bond with concrete. CFRP bar equivalents were placed on the concrete surface of the confined zone having a cross-sectional area equivalent to the tributary area of the CFRP wraps used in the tests. Support points were restricted in z ($u_z=0$).

The beam mesh comprised 50mm brick elements while the loading plate and support consisted of 50mm tetrahedral elements. Beams 3, 4 and 5 had a finer mesh of 25mm brick elements in the potential plastic hinge region to closely study the behavior of the beam confined by CFRP.

Displacements were prescribed in increments of a 1mm step in the middle of the top surface of the loading plate. Standard Newton-Raphson iteration was used until attainment of nominal capacity, then the stepping algorithm was changed to Standard Arc Length.

Monitoring Points

Two monitoring points were used to plot the load displacement curves: one was located in the center of the cross-section at the bottom surface of the beam at midspan. Another monitoring point was placed on the loading plate to read the reaction.

Analysis

Finite element analysis of the beams under increasing monotonic displacement was carried out in order to compare load-nominal drift envelopes as shown in Figure 9. Response was also calculated under the cyclic load history, however, when compression reinforcement attained instability conditions convergence became very precarious. Figure 11 plots the results for the cyclic load-displacement hysteretic loops of beams 1 to 5; up until convergence was possible, the models reproduced adequately load – displacement envelope. Even better is the ability of the simulation to reproduce the observed damage patterns, strain penetration in the longitudinal reinforcement over the shear span and the disintegration of the flanges (see Figures 10, 12-15).

Figures 12 (a) and (b) plot the calculated longitudinal reinforcement strains over a distance from beam midspan to the left support, under hogging and sagging moments, respectively. Loading plate locations are also marked in the figure by the vertical black line. Drift levels noted in the two figures (2.6% and 5.4%) correspond to the last point of convergence in the solutions, and are actually nominal values, i.e. they are obtained as the ratio of loading point displacement divided by the shear span length. The horizontal black lines in the figures correspond to the strain values at bar yielding, calculated from Eq. (2):

$$\varepsilon_y = f_y/E_s \tag{1}$$

i.e., 2.6×10^{-3} and 2.75×10^{-3} according to the f_y values given for top and bottom bars (Table 2). Thus, despite the strength envelope of Fig. 6, strains in the shear span adjacent to the central region have gradually increased to levels that exceed yielding – this process, known as strain penetration has been used to define the notion of the plastic hinge length in recent studies [4]. It is interesting to observe that the true plastic hinge length which equals the length of yield penetration spread over a distance of $l_p=125mm$ (about $0.5d$ for hogging) and $l_p=150mm$ (about $0.6d$ for sagging moments).

The result in Figure 12 (a) and (b) are also consistent with the share of total drift owing to rotation in the central region: experimental values are depicted in Figure 10 at the peak points of the displacement ductility levels applied in the tests. Note that the greater the magnitude of this rotation, the greater the magnitude of average curvature φ that has developed in the confined central region (total length L_c), since from the kinematics of the problem, the curvature distribution under constant flexural moment is also constant and may be calculated from Eq. (1):

$$\theta = \varphi \times 0.5L_c \tag{2}$$

It is observed that the values of θ are generally greater in Beams B1 and B2 where the confinement of the central region

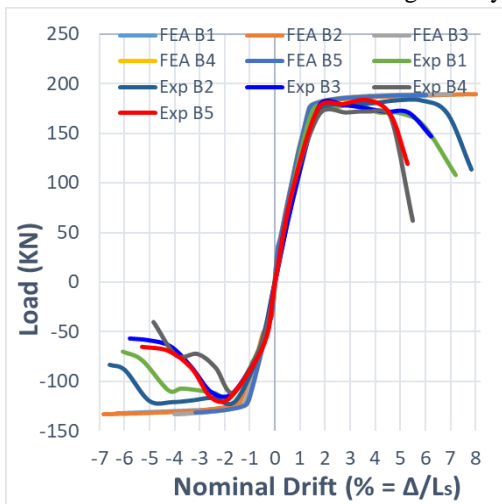


Figure 9 Finite Element Analysis and Experimental Backbone Curves

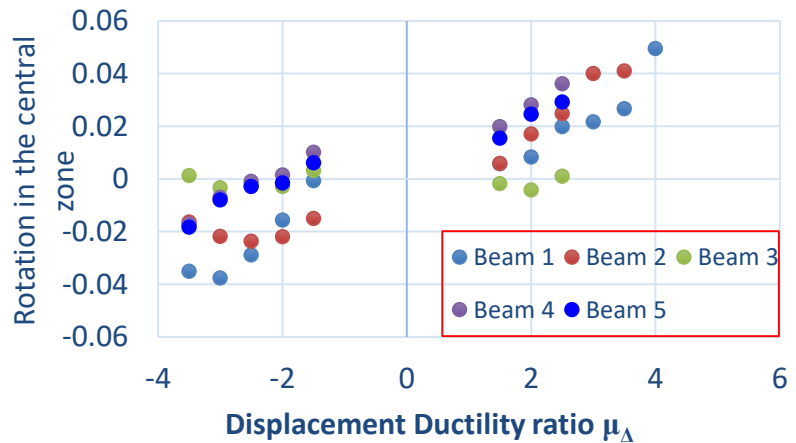


Figure 10: Rotation demand, θ , in the central region of the specimens during testing to different displacement ductility levels.

is the least, reaching values over 4% ductility ratios, which in terms of damage are excessive (local average curvature in the range of 0.1/m), while no yield penetration is occurring in these specimens. On the other hand, in beams B3, B4 and B5, where rotations in the central spans are contained to levels below 2%, significant amount of penetration of yielding is observed.

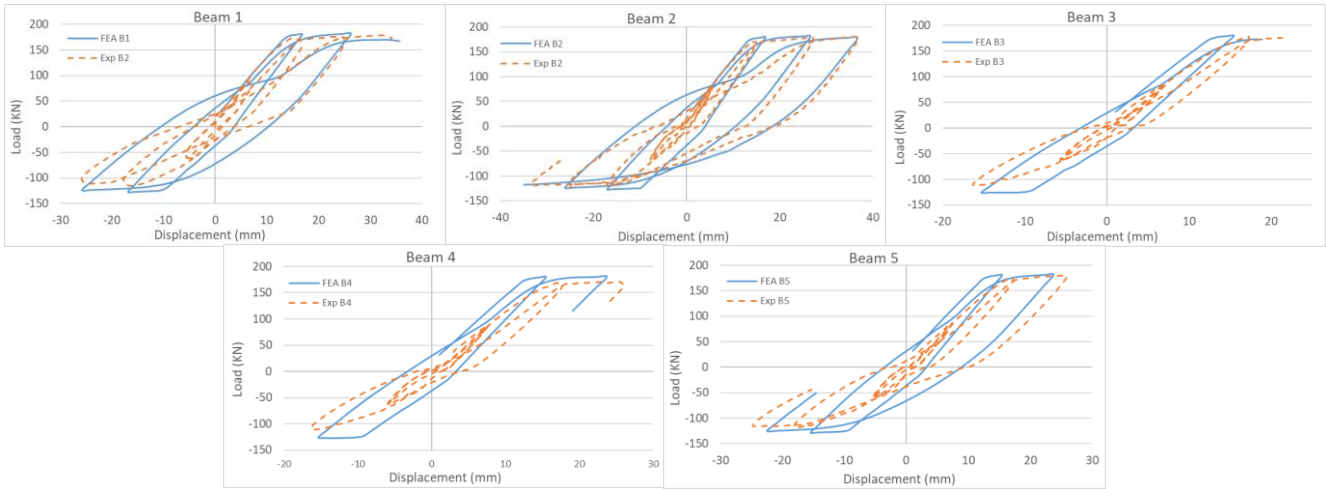


Figure 11 Experimental and Analytical Cyclic Load Displacement Hysteretic curves of beams 1 to 5.

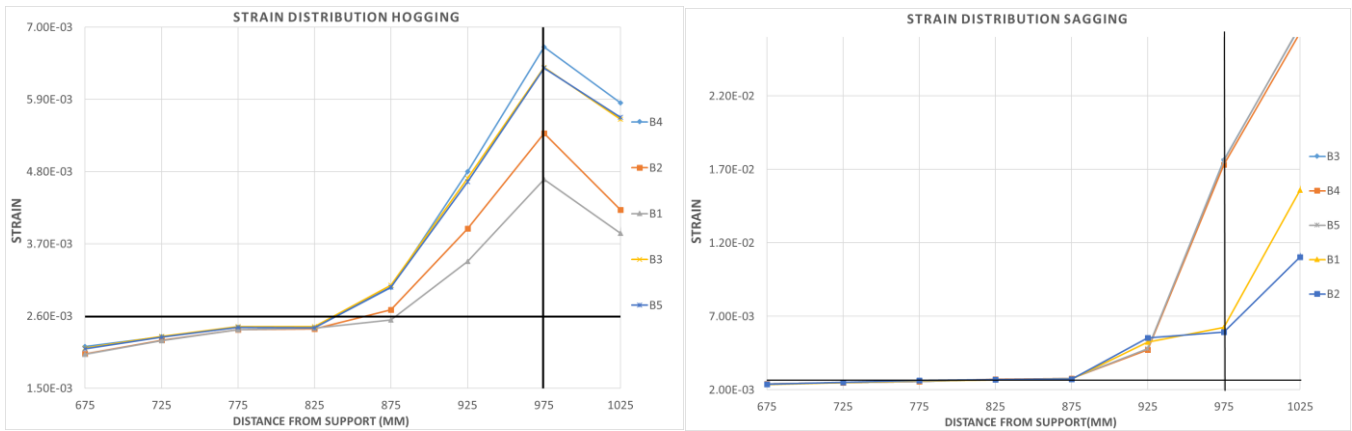


Figure 12a Strain Distribution of Beams 1 to 5 for Hogging Nominal Drift $\Delta=2.6\%$

Figure 12b Strain Distribution of Beams 1 to 5 for Sagging Nominal Drift $\Delta=5.4\%$

Regions of large bar tensile strains or beam curvature correspond to significant residual strains upon reversal of the imposed displacement. Residual strains correspond to open cracks and this is why in the next cycle buckling occurred as observed in both experiment and analysis, as depicted in Fig. 8, and Fig. 13 and 14 which plot the analytical results. Note the difference in the state of the bars at $\mu=2$ when bars buckled only in beam B1 and were restrained in beam B2 due to the close spacing of stirrups.

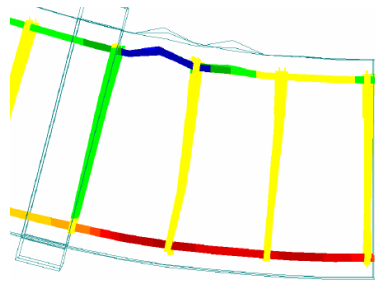


Figure 13(a) Buckled bars in beam B1 at nominal displacement ductility $\mu=2$

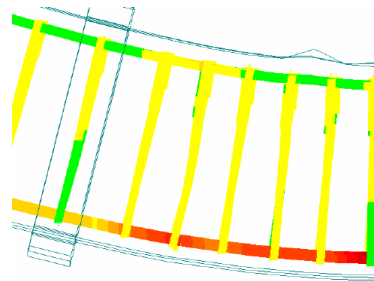


Figure 13(b) Bars in beam B2 at nominal displacement ductility, $\mu=2$

During Testing, all beams developed diagonal cracks in the flange near supports as shown in Figure 14. This occurred due to the shear flow that develops as a result of the kinematic requirements of compatibility at the slab beam interface (where shear transfer occurs from slab to web), exacerbated by the fact that the flanges were free of stress in the ends of their effective width. The same behavior is also evident in the F.E. simulation depicted in Figure 15.



Figure 14 Diagonal cracks in the flange from the experimental program – top view

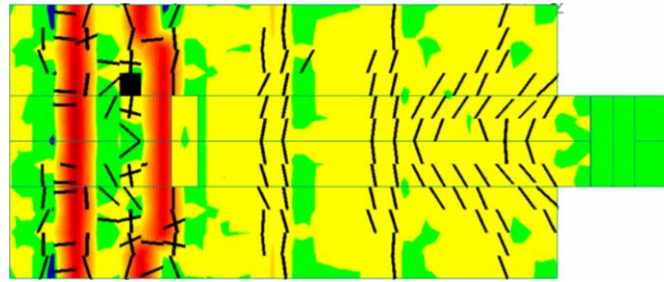


Figure 15 Cracks in the flange simulated on ATENA - top view

CONCLUSIONS

The experimental program illustrates a number of important aspects of behavior in reinforced concrete under displacement reversals which are often obscured by the emphasis of concrete design on load, rather than deformation demand. Five beams were tested under symmetric load, all having greater flexural strength in the shear spans as compared to the central region where flexural demand is maximum. Under standard stirrup arrangement designed according with the non-seismic requirements for stirrup placement of ACI 318 [1] the weakened region developed excessive localized damage with local rotation demands in the excess of 4%, and commensurate slip of longitudinal reinforcement in that location. This was partly mitigated by the addition of confinement by placing denser stirrups and was totally suppressed through CFRP jacketing; in this manner, confinement increased significantly the anchorage strength of the primary reinforcement in the weakened region to the extent that bar slip was minimal in that region, with the total drift capacity owing to spread of post-yield bar strains in the flexurally stronger shear spans. Plastic hinging occurred in these circumstances extending beyond a length of about $0.5d$, where d is the effective depth of the member. This represents the state of reinforcement yielding and penetration thereof in the shear span of columns where ample anchorage strength is provided at the footing support. The experiments were simulated using an advanced nonlinear Finite Element platform illustrating that it is possible to obtain localized damage phenomena and mechanistic insights under cyclic loading through analysis with great confidence.

ACKNOWLEDGMENTS

The first and second authors would like to thank SIKA Near East for providing the material needed. Analysis was done at York University under an OTS scholarship award to the first author. Computational facilities were provided by York University.

REFERENCES

- [1] American Concrete Institute (ACI), Building Code Requirements for Reinforced Concrete (ACI 318-and commentary ACI318M-14), Detroit, Michigan, 2014
- [2] ATENA Program Documentation, Cervenka Consulting, Prague, Czech Republic, 2007.
- [3] CEB-fib, Bond of reinforcement in concrete. Bulletin 10, fib Bulletin (Vol. 10), 2000.
- [4] K. G. Megalooikonomou, S. P. Tastani, and S. J. Pantazopoulou, "Effect of yield penetration on column plastic hinge length," 2017.